ORIGINAL ARTICLE

Adsorption of Congo red and malachite green using H_3PO_4 and NaCl-modified activated carbon from rubber (*Hevea brasiliensis*) seed shells

Chinenye Adaobi Igwegbe[1] · Joshua O. Ighalo[1,2] · Kenechukwu Keluo Onyechi[3] · Okechukwu Dominic Onukwuli[1]

Abstract

Cationic dyes are toxic environmental pollutants that need to be mitigated from the aqueous environment. In this study, *Hevea brasiliensis* seed shells (HBSS) activated with H_3PO_4 (PHBSS) and NaCl (SHBSS) were explored for the removal of Congo red (CR) and malachite green (MG) from their aqueous solutions. The adsorbents were carbonised at 300 °C for 3 h and characterised by FTIR, SEM and XRF. Maximum removals for CR and MG were observed at pH 2 and pH 10, respectively. The uptake of both dyes was optimum at 0.3 mm particle size, 2 g/L adsorbent dosage and 100 mg/L initial dye concentration. The adsorption capacity of PHBSS and SHBSS to CR was 55.87 and 50.51 mg/g, respectively, while for MG was 58.48 and 56.82 mg/g, respectively. The study observed that the uptake of both dyes by both adsorbents was best fit to the Freundlich isotherm and the pseudo-second order kinetic model. The thermodynamics modelling revealed that the process was spontaneous and endothermic. The mechanism of CR and MG uptake was by a combination of electrostatic attraction, π–π electron–donor interaction, hydrogen bonds and pore diffusion. Furthermore, H_3PO_4 was a better activating agent for HBSS than NaCl given the current application.

Keywords Adsorption · Congo red · Malachite green · Thermodynamics · Textile wastewater

Abbreviations

AC	Activated carbon
AWWA	American Water Works Association
CR	Congo red
FTIR	Fourier transforms infrared spectroscopy
HBSS	*Hevea brasiliensis* Seed shells
MG	Malachite green
PHBSS	H_3PO_4-treated HBSS activated carbon
SHBSS	NaCl-treated HBSS activated carbon
UHBSS	Unmodified HBSS activated carbon
SEM	Scanning electron microscopy
XRF	X-ray fluorescence

✉ Chinenye Adaobi Igwegbe
  ca.igwegbe@unizik.edu.ng

✉ Joshua O. Ighalo
  oshea.ighalo@yahoo.com

1   Department of Chemical Engineering, Nnamdi Azikiwe University, PMB 5025, Awka, Nigeria

2   Department of Chemical Engineering, University of Ilorin, PMB 1515, Ilorin, Nigeria

3   Department of Pharmaceutics and Pharmaceutical Technology, Nnamdi Azikiwe University, Awka, Nigeria

Introduction

Textile, food, cosmetic and pharmaceutical businesses release fairly treated or untreated waters to the environment which may result in the pollution of the receiving waters (Ahmadi et al. 2020; Mesbah et al. 2020). These wastewaters may impede aquatic live (including plants and animals) (Abdullahi et al. 2020). The consumption of water containing a trace or low concentration of dye is unsafe for different usages (Louis and Thomas 2013). Untreated water can result in un-aesthetic conditions in the received water (Ighalo and Adeniyi 2020b). The overall consumption of dye by the textile business globally is above 10^7 kg per year (Hessel et al. 2007). Anionic dyes possess a negative charge, while cationic dyes like congo red (CR) and malachite green (MG) possess a positive charge in aqueous solutions and are toxic to the environment than the anionic dyes (Dahiru et al.

2018; Igwegbe et al. 2020a; Kumari et al. 2020; Rehman et al. 2020).

Many methods have been applied for dye uptake from aqueous media (Gupta 2009; Sharma et al. 2011); that can be grouped into chemical, physical and biological processes. Adsorption, which is a physical technique is the most common method for the reduction of colour and other toxic chemicals from the aqueous environment due to its high efficiency, low cost, simple operation and less advanced equipment required (Balarak et al. 2021a; De Gisi et al. 2016; Uddin 2017).

Hevea brasiliensis (Rubber) seed shells (HBSS) is an agro-waste discharged to the environment as unwanted material by rubber processing. The rubber tree is widespread in the northern part of South America and was introduced into Africa and South-East Asia (Blagodatsky et al. 2016). It can withstand waterlogged and dry areas. It can grow on volcanic, peaty and acidic soils. These seeds are abundantly obtainable and can serve as an alternative to synthetic adsorbents. Activated carbon (AC) production from unwanted matter is of environmental and economic importance (Igwegbe et al. 2020b; Onyechi 2014). Bio-based adsorbents are more advantageous than chemically synthesised adsorbents since they are less toxic, renewable, cheaper to process and simple preparation method (Sud et al. 2008).

Hevea brasiliensis seed shells (HBSS) have not been explored as a potential adsorbent for the uptake of cationic dyes like CR and MG. This study explores this gap in knowledge to examine the suitability of H_3PO_4 and NaCl as an activating agent for this specific application. To this effect, HBSS activated with H_3PO_4 and NaCl were tested for the removal of two common dyes, congo red (CR) and malachite green (MG) from their aqueous solutions. Also, the impact on the process of changes in pH, adsorbent particle size, adsorbent dosage, initial dye concentration, contact time and temperature were considered. The isotherm, thermodynamics, kinetics and the activation energies of the process was also studied. The mechanism of the dye uptake was also explored.

Materials and methods

Materials

Congo red (maximum absorption capacity, $\lambda_{max} = 419$ nm, molecular weight = 696.66 g/mol and chemical formula = $C_{32}H_{22}N_6Na_2O_6S_2$) and malachite green ($\lambda_{max} = 617$ nm, molar mass: 364.911 g/mol and chemical formula = $C_{50}H_{52}N_4O_8$) synthesised by LOBA Chemie PVT LTD., India were of analytical grade. The molecular structures of both adsorbates are presented in Fig. 1. *Hevea brasiliensis* seed shells (HBSS) were collected from the Rubber Research Institute of Nigeria, Benin.

Adsorbent preparation

Hevea brasiliensis seed shells (HBSS) were cleaned with distilled water, dried in the oven at 105 °C for 8 h and ground. The ground material was stored in a container. The H_3PO_4-treated HBSS AC (PHBSS) was prepared by soaking some portion of HBSS in 60% H_3PO_4 acid in the wt ratio of 1:1 for 24 h at 27 °C. Then, the treated sample was carbonised at 300 °C for 3 h using muffle furnace (Model SX-2.5-10), cooled, washed with distilled water until pH 7 is reached and filtered (Igwegbe et al. 2020a). The cake was dried for 8 h at 105 °C in the oven, cooled and sieved to different particle sizes (0.3–1.5 mm), and stored in airtight containers for the sorption experiments. The NaCl-treated HBSS AC (SHBSS) was prepared by soaking some portion of HBSS in 60% NaCl in the wt ratio of 1:1 for 24 h at 27 °C. The same procedure reported for PHBSS was repeated for SHBSS preparation. The SHBSS was separated into different particle sizes (0.3–1.5 mm) and stored in airtight containers for the sorption experiments. For the 'untreated'
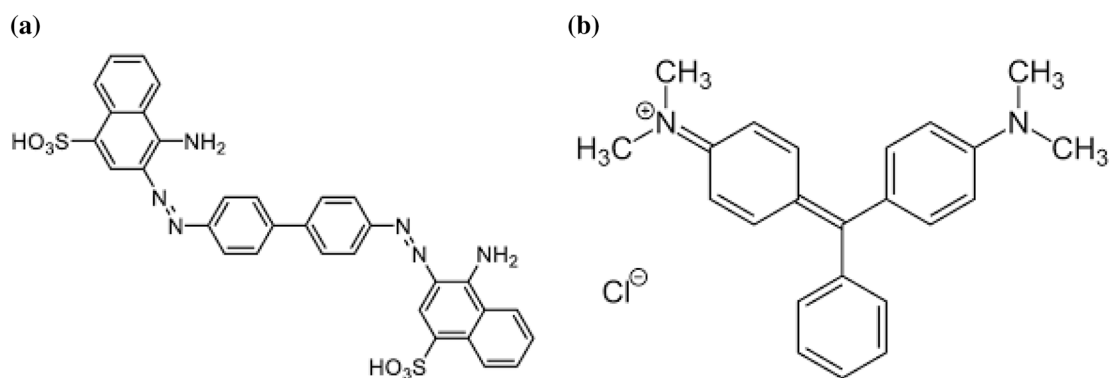
Fig. 1 Structure of congo red (**a**) and malachite green (**b**)

carbon (UHBSS), a portion of the HBSS was not treated with any chemical agent and the same procedure reported for PHBSS was repeated for UHBSS preparation.

Adsorbents properties

The activated carbons (PHBSS and SHBSS) characteristics were determined to observe their respective properties. X-ray Fluorescence (XRF) spectrometer (Munipal 4 model) was utilised to quantify the oxides present in the UHBSS, PHBSS, and SHBSS. The functional groups present in UHBSS, PHBSS, and SHBSS were acquired using a Shimadzu S8400 FTIR spectrophotometer (in the range of 4000–400 cm^{-1}). Surface morphology of UHBSS, PHBSS, and SHBSS was determined via the SEM (Scanning Electron Microscopy). 3D reconstruction of the adsorbent surface based on SEM images was done using ImageJ v1.53 (Ighalo et al. 2021).

Adsorption studies

The adsorption experiments were performed using 100 mL of dye stock solution of different concentrations (100–500 mg/L) prepared by dispersing a measured mass of dye powder in deionised water of known volume. The solution's pH was adjusted between 2 and 10 with 0.1 M HCl or NaOH in the flasks and a measured mass of biosorbent (0.2–2.0 g/100 mL) with a specific particle size (0.3–1.5 mm) was introduced. The mixture was treated for the desired period (10–150 min) at 120 rpm and at a specific temperature (30–70 °C). Then, the treated and centrifuged solution was measured for its new concentration using a UV–vis spectrophotometer (Model UV 754) at CR$_{\lambda max}$ of 419 nm and MG$_{\lambda max}$ of 617 nm. The amount of CR and MG adsorbed per unit weight of sorbent (mg/g) was gotten via Eq. 1

$$q_e = \frac{(C_o - C_e)V}{W}, \tag{1}$$

where C_0 is the initial CR or MG concentration in the solution (mg/l); C_e is the final CR or MG concentration in the solution (mg/l); V is the volume of the adsorbate sution (l), and W is the weight of the adsorbent (g).

The percentage CR and MG removal, E (%) was estimated for each run by Eq. 2

$$E(\%) = \frac{Co - Ce}{Co} \times 100. \tag{2}$$

Results and discussions

Adsorbent characterisation

Physicochemical properties

Physicochemical properties of PHBSS and SHBSS were determined by various methods stated in literature and summarised in Table 1. Though most of the properties of both AC were similar, there were significant differences in other properties like the iodine number. A high value of fixed carbon was obtained for PHBSS and SHBSS. This is expected as the carbonisation process has driven out much of the volatile matter from the biomass source. The iodine number is a measure of the pore volume of the adsorbent (Saka 2012). The iodine number and bulk density recommended as the minimum by the American Water Works Association (AWWA) for AC to be used in the removal of low molecular weight compound is 500 mg/g and 0.25 gm/mL respectively (Devi et al. 2012). The values of iodine number and bulk density for PHBSS and SHBSS exceed the minimum requirements hence their suitability as adsorbents. The pH values are near neutral which shows that the carbons can also be applied for the purification of drinking water (Baseri et al. 2012). However, that activated with phosphoric acid had a pH value of 6.6 while that activated by sodium chloride (a normal salt) has a pH value of 7.1. The low ash contents (5.14 and 6.05 for PHBSS and SHBSS, respectively) suggests that they can be utilised for the sorptive removal of the dyes from aqueous media (Devi et al. 2012). The specific surface area of PHBSS and SHBSS was 999 and 735 m^2/g respectively. These are relatively high values and reinforces their potential as an adsorbent material for pollutant uptake from aqueous media (Gregg and Sing 1982).

Table 1 Physicochemical properties of the different activated carbon

| Parameter	PHBSS	SHBSS	Method used
Moisture content (%)	3.0	4.0	Rengaraj et al. (2002)
Volatile matter (%)	12.32	12.26	Nwabanne and Igbokwe (2012)
Ash content (%)	5.14	6.05	Ekpete and Horsfall (2011)
Fixed carbon (%)	82.54	81.69	Nwabanne and Igbokwe (2012)
pH	6.6	7.1	Egwaikhide et al. (2007)
Iodine number (mg/g)	878	695	Ekpete and Horsfall (2011)
Bulk density (g/cm^2)	0.55	0.54	Devi and Mishra (2019)
Surface area (m^2/g)	999	735	Nwabanne and Igbokwe (2012)

Table 2 XRF results of HBSS, PHBSS and SHBSS

Chemical constituent	Composition (%)		
	UHBSS	PHBSS	SHBSS
SiO_2	9.06	7.23	7.01
P_2O_5	11.0	11.4	6.50
SO_3	2.00	1.00	0.80
Cl	0.30	3.40	8.45
K_2O	17.3	8.20	12.8
CaO	47.3	46.9	41.3
TiO_2	0.35	0.31	0.83
MnO	0.18	0.75	1.50
Fe_2O_3	3.59	29.9	12.0
NiO	0.19	0.37	0.50
CuO	0.44	1.20	1.70
ZnO	0.22	0.20	0.76
Rb_2O	0.64	0.12	0.05
Ag_2O	4.30	5.50	4.00
Eu_2O_3	0.90	0.30	0.40
BaO	0.38	0.97	2.20
Re_2O_7	0.69	1.70	0.60

Compositional analysis

The chemical composition of the UHBSS, PHBSS, and SHBSS is shown in Table 2. The results obtained reveal that there were changes in the inorganic content of the AC. Potassium oxide (K_2O), ferric oxide (Fe_2O_3), phosphorus oxide (P_2O_5) and calcium oxide (CaO) were the major inorganic components in both the UHBSS, PHBSS, and SHBSS while others were present in smaller amounts. The existence of these inorganics will support the ion adsorption process (Granados-Correa et al. 2013; Igwegbe et al. 2020b).

Functional group analysis

FTIR was used for the identification of the functional groups on UHBSS, PHBSS, and SHBSS. The FTIR spectra of UHBSS, PHBSS, and SHBSS are shown in Fig. 2a–c and summarised in Table 3. The changes in the observed functional groups indicate the modifications that occurred in the adsorbent during the acid and/or salt activation process. These changes were in the form of band shifting and changes in band intensity. For example, the H–C–H asymmetric and symmetric stretch bond assigned to alkane functional groups, which is between frequencies of 2800–3000 cm^{-1} disappeared from the HBSS after acid and salt treatment.
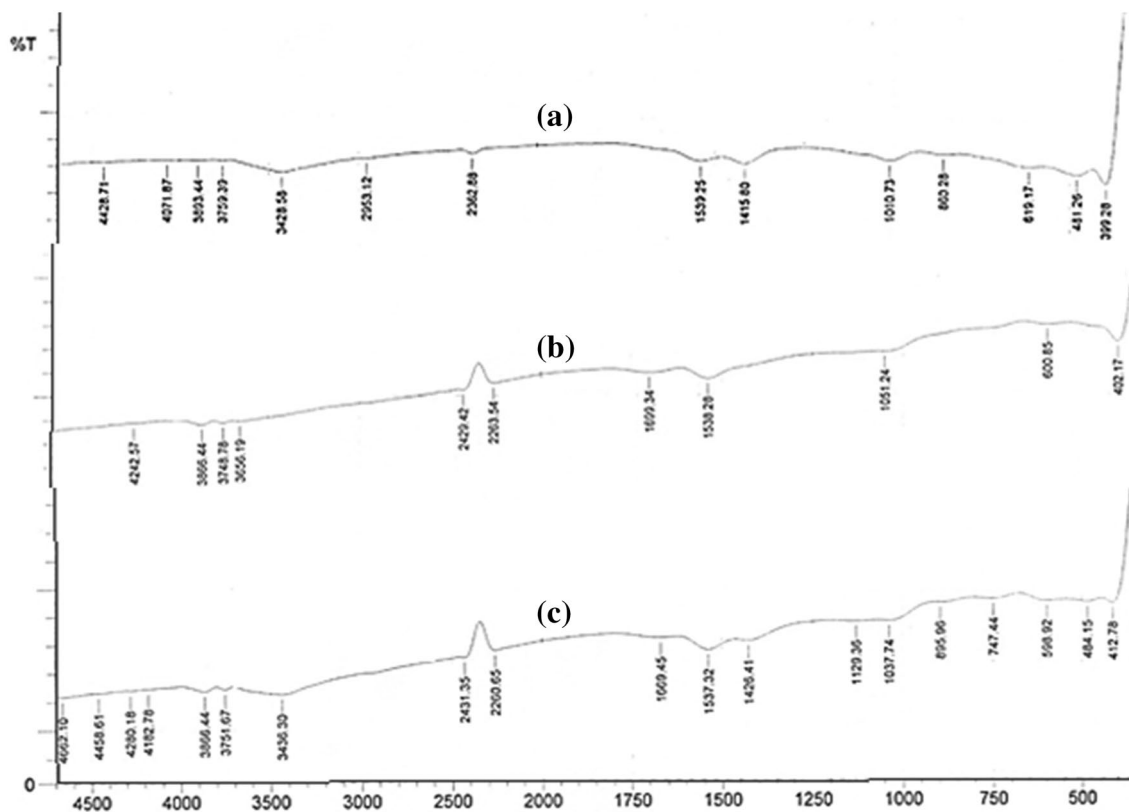
Fig. 2 FTIR spectra of **a** UHBSS, **b** PHBSS and **c** SHBSS

Table 3 FTIR peaks for UHBSS, PHBSS, and SHBSS

Wave number (cm^{-1})			Bond source	Functional group	Description of peak
UHBSS	PHBSS	SHBSS			
619.17	600.85	598.92	C–Br stretch	Alkyl halides	Medium
–	–	747.44	C–Cl stretch	alkyl halides	Medium
860.28	–	895.96	=C–H bend	Alkenes	Strong
1010.73	–	–	C–O stretch	Alcohols, carboxylic acids, esters, ethers	Strong
–	1051.24	1037.44, 1129.36	C–N stretch	Aliphatic amines	
1415.8	–	1426.41	C–C stretch (in ring)	Aromatics	Medium
1539.25	1538.28	1537.32	N–O asymmetric stretch	Nitro compounds	Strong
–	1699.34	1669.45	C=O stretch	Amides, ketones, aldehydes carboxylic acid, esters	Strong
2362.88	2263.54, 2429.42	2260.65, 2431.35	–C≡C– stretch	Alkynes	Narrow and strong
2953.12	–	–	H–C–H asymmetric and symmetric stretch	Alkanes	medium
3428.58	3425.69	3436.30	O–H stretch, H–bonded	Alcohols and phenols	Strong and broad
3759.39, 3893.44	3656.19, 3748.78, 3866.44	3751.67, 3866.44	O–H stretch, free hydroxyl	Alcohols and phenols	Strong and sharp

From the analysis, the presence of functional groups such as alkyl halides, alkanes, aliphatic amines, alcohols, alkynes, nitro compounds, carboxylic acids, phenols, esters and ethers were confirmed. The most abundant type of functional group on the AC is the O–H stretch in alcohols which is a very strong and broadband (Souza et al. 2021). The attack on the O–H functional group during the activation process was confirmed by the reduction in the O–H vibration stretches on the spectrum. In using up the oxygen, the activation process helped to create more pores in the final product. The peak at 1550–1475 cm^{-1} corresponds to the N–O asymmetric stretch (nitro compounds). The effect of the hydroxyl group is more intense because of the hydrogen bonding with other hydroxyl bonds since they do not exist in isolation forming a stable structure (Coates 2010; Igwegbe et al. 2016).

Morphological analysis

The SEM micrograph of UHBSS, PHBSS, and SHBSS are shown in Fig. 3a–c at a magnification of 4000×. From the micrograph, the thread-like nature of the carbons can be observed alongside dotted illuminations. There were numerous cavities and undulations on the surface of the AC thereby giving it a heterogeneous outlook. It can also be observed from the micrographs that the acid and salt activation improved the porosity of the carbon by increasing the surface heterogeneity. The greater surface heterogeneity of the activated carbons suggests a greater likelihood for better adsorptive performance by the material (Ighalo and Adeniyi 2020c) due to the presence of numerous features and subsequent increase in specific surface area. For a better analysis of the adsorbent surface, the SEM images (which gives a

vertical view) were reconstructed to 3D images (Ighalo et al. 2021) and shown in Fig. 4a–c. It can be observed from the 3D morphological images that the adsorbent surface was more deeply gouged and ridged after chemical modification. Though the surface was ridged, the valleys represent areas where the openings exist for convoluted cavities within the adsorbent microstructure.

Effect of process variables on adsorption

Effect of pH

The effect of pH (2–10) on the adsorption of CR and MG at a contact time of 60 min is shown in Fig. 5. It can be observed that the adsorption process for both CR and MG is pH-dependent. However, the behaviour of the adsorption process with pH change was very different for CR and MG. CR uptake was highest at pH 2 and decreased continually till pH 10 while MG uptake was lowest at 2 and increased continually till pH 10. These were the optimum pHs utilised for the rest of the study. Higher uptakes of both CR and MG were observed at pH of 2 and 10, respectively for all adsorbents. The pKa of CR is 4.1 and it is protonated to its cationic (positively charged) form below this pH. It is therefore not surprising that uptake was high at low pH and reduced with increase in pH where the adsorbent was neutral. The pKa of MG is 10.3. Below this value, it is protonated and exists in its cationic (positively charged) form. At lower pH, H$^+$ competes for MG in solution thereby reducing its uptake (Gautam et al. 2015). However, as pH increases, there is an observable increase in MG uptake as this competition increases. Optimum uptake of MG at pH 10 was 99.6%
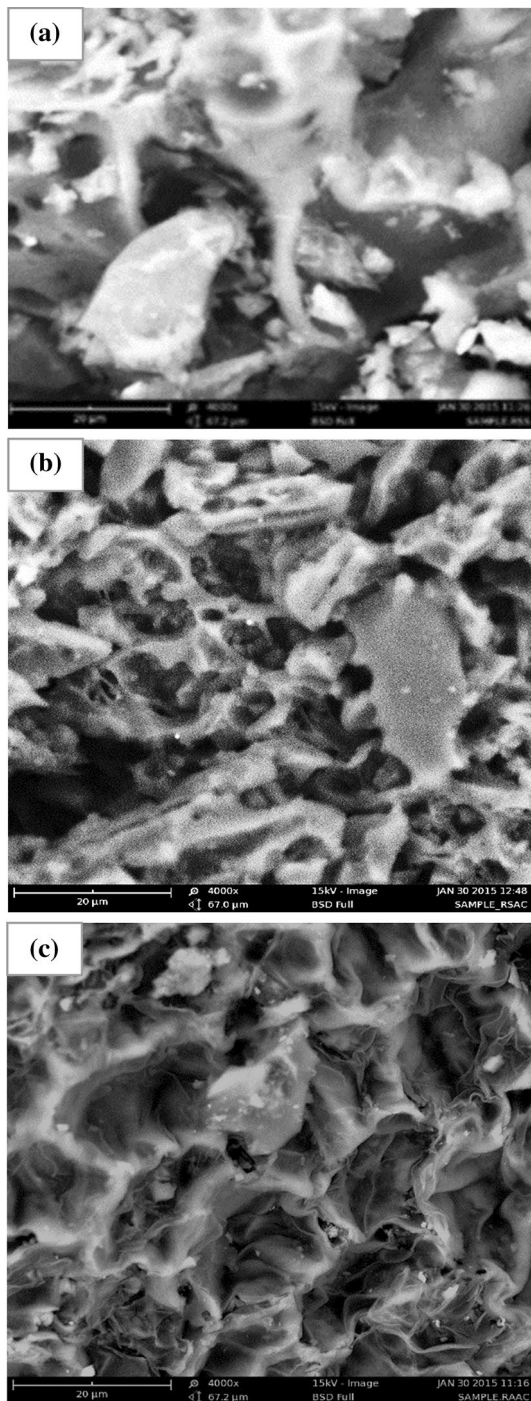
Fig. 3 SEM images of **a** UHBSS, **b** PHBSS and **c** SHBSS

and 99.4% for PHBSS and SHBSS, respectively. Optimum uptake of CR at pH 2 was 97.0% and 96.7% for PHBSS and SHBSS, respectively. The favourability of low pH (pH 2) to CR adsorption and high pH (pH 10) have been observed for Fe–Zn bimetallic nanoparticles (Gautam et al. 2015). Also, the favourability of high pH to MG adsorption have been observed for anaerobic granular sludge (Cheng et al. 2008),

AC from jute fibres (Porkodi and Kumar 2007) and chitosan-coated bentonite (Wan Ngah et al. 2010).
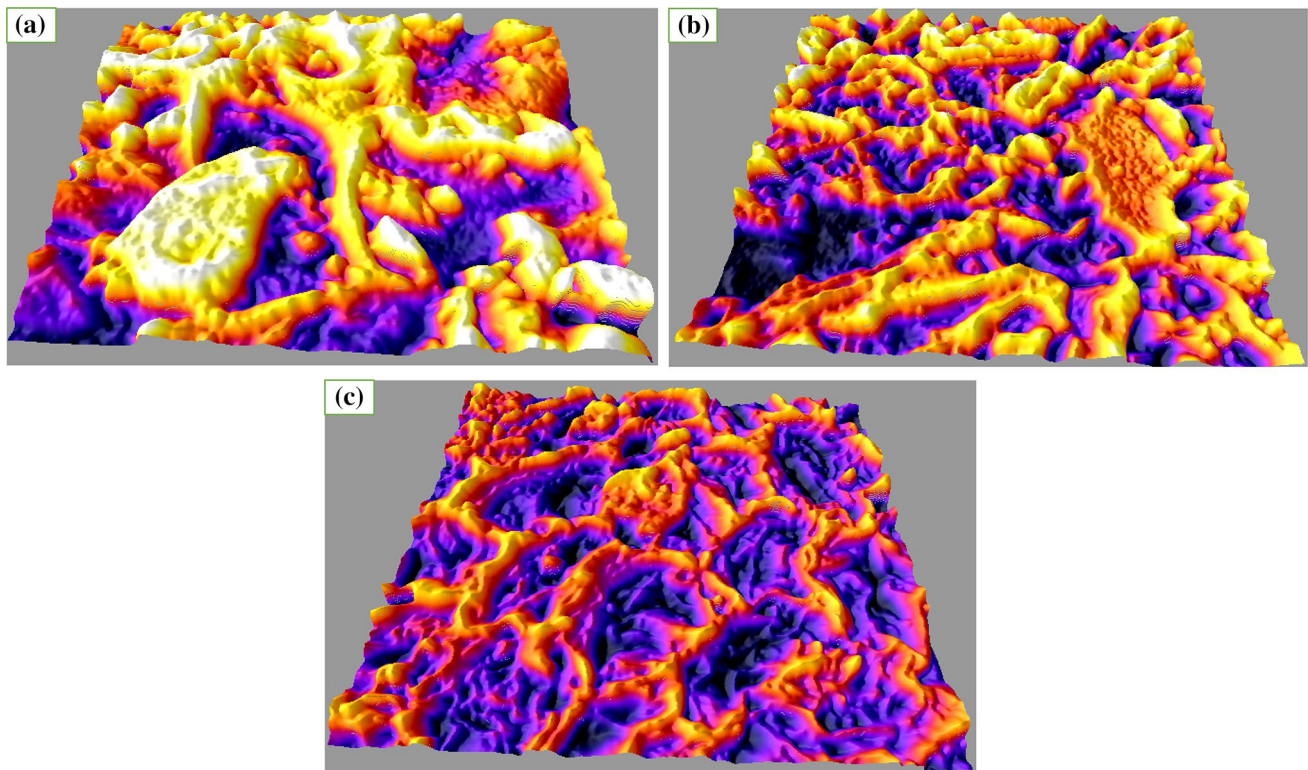
Effect of particle size

The influence of particle size (0.30, 0.60, 0.85, 1.00, and 1.50 mm) on the uptake of CR and MG onto PHBSS and SHBSS was studied and shown in Fig. 6. The pH was retained at that of the original solution without any adjustment. Figure 6 shows that increase in the adsorbent particle size reduced the percentage removal of CR and MG. This could be due to the reduced access to active sites and an overall reduction in surface area that is associated with larger adsorbent particles (Igwegbe et al. 2016). Also, from Fig. 6, it was seen that the PHBSS performed best for CR and MG removal yielding 58% and 90% removal, respectively at 0.3 mm particle size. A similar effect of particle size was also observed by other researchers for biochar from peanut hull (Han et al. 2016), biosorbent from neem sawdust (Khattri and Singh 2009) and AC from coconut shell (Aljeboree et al. 2017).

Effect of dosage of adsorbent

The effect of adsorbent dosage on the removal of CR and MG was studied by varying the dosage of adsorbent (0.2, 0.5, 1.0, 1.5, and 2.0 g/100 mL) at optimum pH and dye initial concentration of 100 mg/L. As seen in Fig. 7, the percentage of CR and MG removals increased sharply with increased dosage up to 1.0 g/L but increased only slightly from 1.0 to 2.0 g/100 mL for all adsorbents. PHBSS performed better than the SHBSS as also observed in other cases. The increase of adsorbent dosage resulted in more availability of active sites for adsorption of the dyes (Eletta et al. 2020b). A similar effect of adsorbent dosage on cationic dye uptake has been observed for AC from jute fibres (Porkodi and Kumar 2007), cocoa AC (Eletta et al. 2021), magnetic hydroxyapatite nano-powder (Zhang et al. 2016) and activated red mud (Tor and Cengeloglu 2006).

Effect of dye initial concentration

To investigate the effect of initial dye concentration on CR and MG uptakes, the concentration was varied from 100 to 500 mg/L at the optimum pH, adsorbent dosage of 2.0 g/l, and contact time of 60 min. As presented in Fig. 8, CR and MG uptake was reduced with increasing initial concentration, being optimum at 100 mg/L for both PHBSS and SHBSS. This may be caused by the oversaturation of the adsorbent with the dye with increasing dye concentration (Balarak et al. 2020, 2021b). A similar effect of initial concentration on cationic dye uptake has been observed for Fe–Zn bimetallic nanoparticles (Gautam et al. 2015).

Fig. 4 3D reconstruction of images of **a** UHBSS, **b** PHBSS and **c** SHBSS surfaces

Fig. 5 Effect of pH of solution on the efficiency of removal of CR and MG (Particle size = 0.30 mm, dosage of adsorbent = 1.0 g/100 mL, dye concentration = 100 mg/L, time = 60 min, temperature = 30 °C)
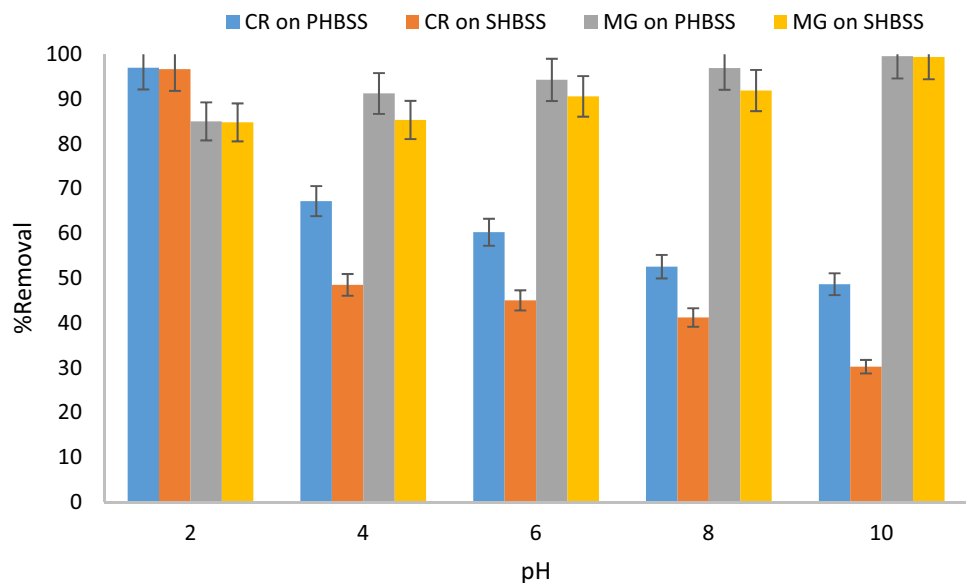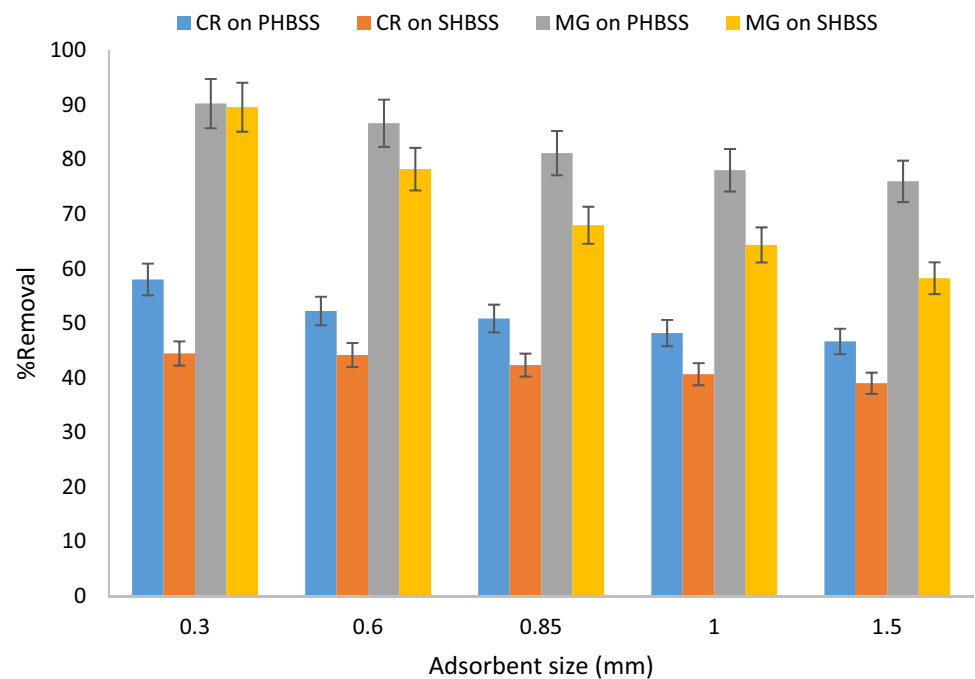

Effect of temperature

As observed in Fig. 9, the percentage adsorbed increased with increasing solution temperature from 30 °C to an optimum of 60 °C at a dye concentration of 100 mg/L and optimum pH. However, it decreased drastically after the optimum temperature. From these observations, it is suggested that the uptakes of both CR and MG is endothermic. This was subsequently confirmed by the thermodynamics study. The increase in the removal efficiencies with temperature is due to the increase in the mobility of the dye molecule with an increase in their kinetic energy (Ahmad and Kumar 2010) hence helping the adsorbate overcome the mass transfer limitation at the solid–liquid interphase (Eletta et al. 2020b).

Fig. 6 Effect of particle size on efficiency of removal of CR and MG (concentration = 100 mg/L, dosage of adsorbent = 1.0 g/100 mL, time = 60 min, temperature = 30 °C)

Fig. 7 Effect of dosage of adsorbent on the efficiency of removal of CR and MG (particle size = 0.30 mm, optimum pH, concentration = 100 mg/L, time = 60 min, temperature = 30 °C)
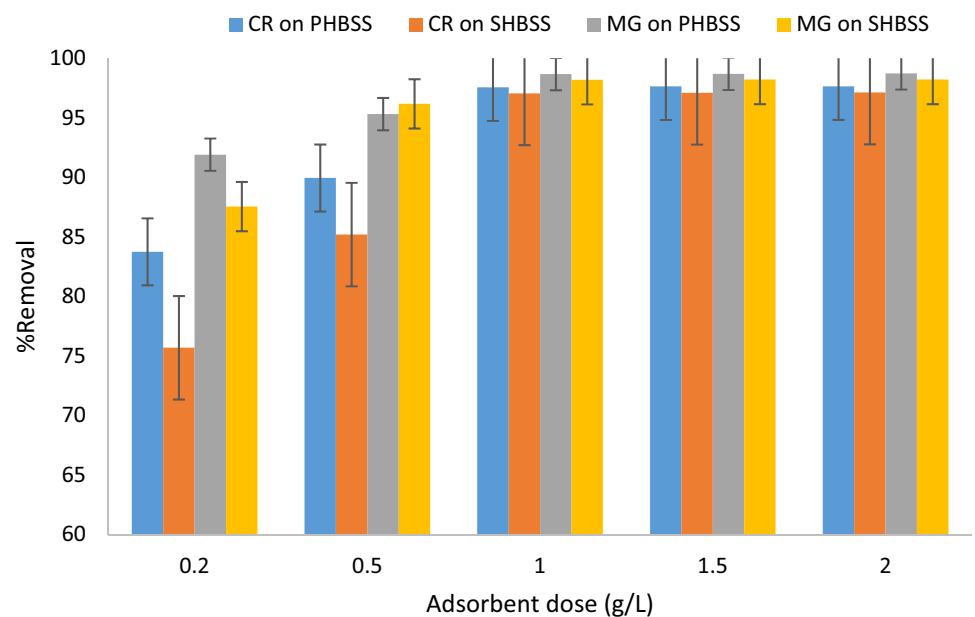

Effect of contact time

Figure 10 presents the influence of contact time on the removal efficiency of CR and MG on PHBSS and SHBSS at a constant initial concentration of 100 mg/L and optimum pH. The efficiency of CR and MG depletion was rapid from 10 to 90 min. Equilibrium was achieved after 90 min and there was no additional dye uptake after that time. At initial contact, the high concentration of dyes in solution helped to provide a mass transfer driving force for the process (Eletta et al. 2020a). Besides, there were lots of unfilled active sites

in the adsorbent. As the contact time increased, the concentration of dye in solution was reduced and more sites in the adsorbent were filled leading to the reduction in the speed of uptake (Ahmadi and Igwegbe 2018). A similar effect of contact time on cationic dye uptake has been observed for Fe–Zn bimetallic nanoparticles (Gautam et al. 2015), chitosan-coated bentonite (Wan Ngah et al. 2010), pine cone biosorbent (Dawood and Sen 2012) and activated red mud (Tor and Cengeloglu 2006).

Fig. 8 Effect of **a** CR and **b** MG concentrations on the % adsorbed (particle size = 0.30 mm, optimum pH, dosage of adsorbent = 2.0 g/100 mL, temperature = 30 °C)
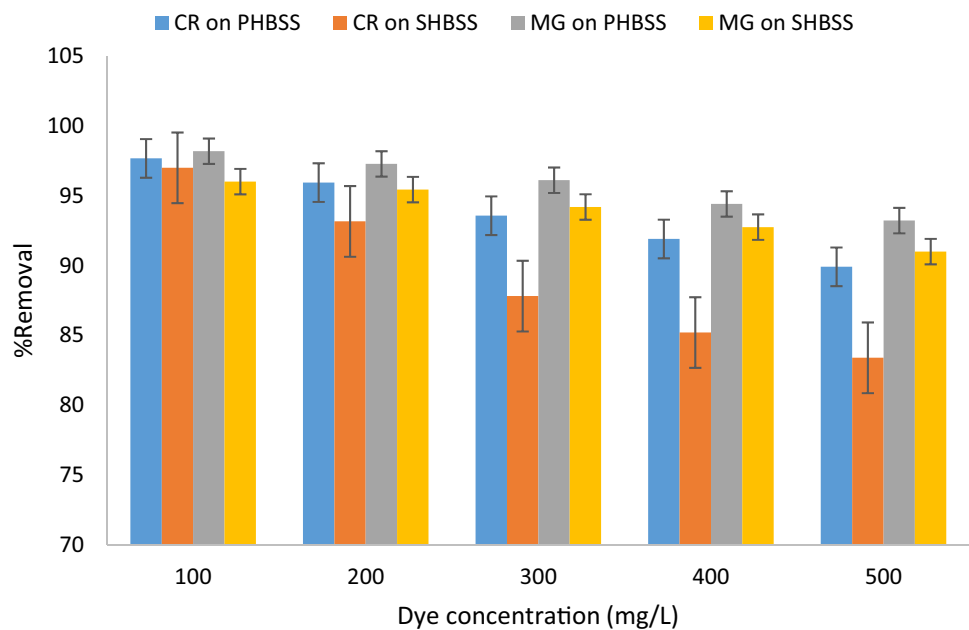
Fig. 9 Effect of solution temperature on the % adsorbed (particle size = 0.30 mm, optimum pH, dosage of adsorbent = 1.0 g/100 mL, dye concentration = 100 mg/L, time = 60 min)
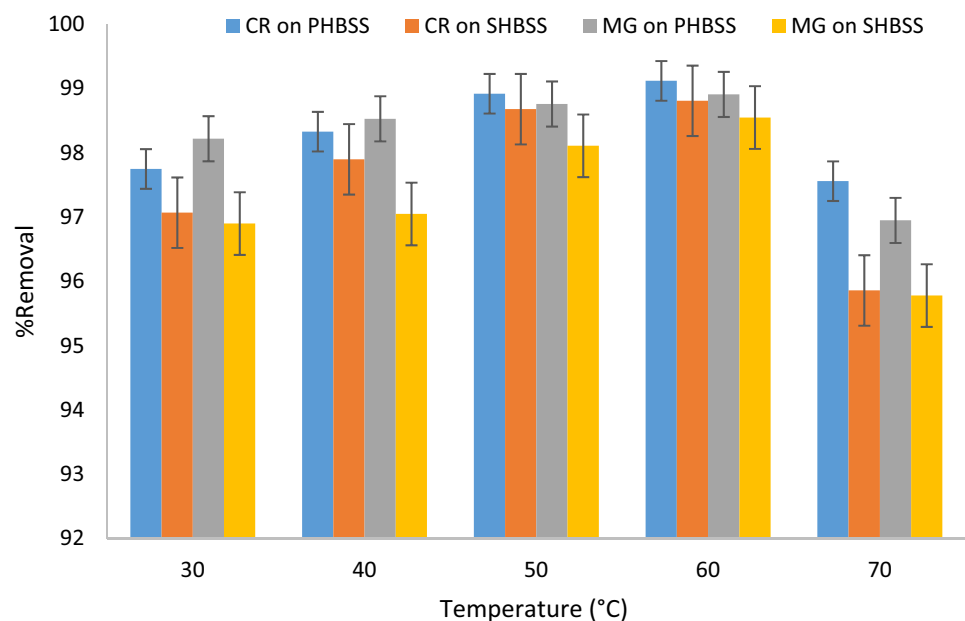

Equilibrium isotherm modelling

The adsorption data were modelled based on the Langmuir (Langmuir 1918), Freundlich (Freundlich 1906), Temkin (Temkin and Pyzhev 1940), Elovich (Elovich and Larinov 1962), Jovanovich (Misra 1973) and Harkin-Jura (Jura and Harkins 1943) isotherms. The plots for the modelling are shown in the Supplementary Material (Figs. S1–S4) and summarised in Table 4. From the values of the coefficient of determination (R^2), it can be observed that the best-fit isotherm for the adsorption of both CR and MG onto PHBSS and SHBSS was the Freundlich isotherm. This suggests that

the adsorption was multi-layer in nature. It also reveals that the surfaces of both adsorbents were energetically heterogeneous (Ahmadi and Igwegbe 2020; Ighalo and Adeniyi 2020a). This is not uncommon for adsorbents prepared by thermochemical processes (Jeirani et al. 2017; Shafeeyan et al. 2010). Furthermore, it is understood from the adsorption process that CR and MG are adsorbed onto stronger binding sites before binding onto sites of lesser energy (Hevira et al. 2020). With a greater degree of site occupancy, the strength of binding decreases. For all four cases of the Freundlich isotherm in Table 4, the n value was greater than 1 suggesting that the adsorption process was favourable

Fig. 10 Effect of contact time and temperature on percentage of CR and MG adsorbed at room temperature (particle size = 0.30 mm, dosage of adsorbent = 1.0 g/100 mL, dye concentration = 100 mg/L, pH = 2 for CR and pH = 10 for MG)
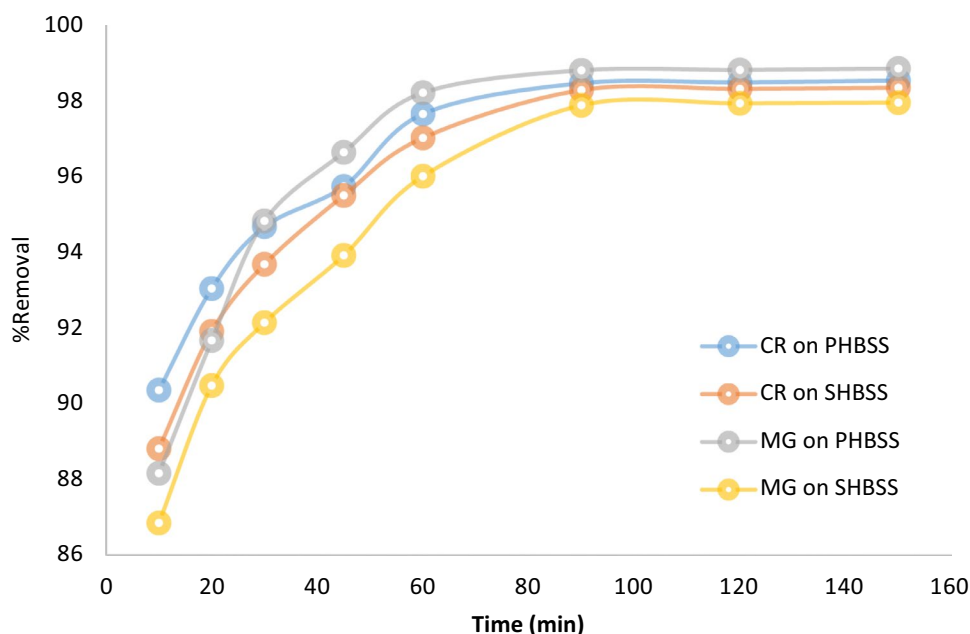
(Ighalo and Eletta 2020). Though the Langmuir isotherm was not the best fit, it was also accurate for modelling the adsorption data (Kumar 2007). The adsorption capacity of PHBSS and SHBSS to CR was 55.87 and 50.51 mg/g respectively while for MG was 58.48 and 56.82 mg/g respectively.

Kinetics modelling

The adsorption data were modelled based on the pseudo-first order (Lagergren and Svenska 1898), pseudo-second order (Ho and McKay 1999; Ho et al. 2000), and intraparticle diffusion kinetic models (Weber and Morris 1963). The plots for the modelling are shown in the Supplementary Material (Figs. S5–S8) and summarised in Table 5. From the values of the coefficient of determination (R^2), it can be observed that the best-fit kinetic model for the adsorption of both CR and MG onto PHBSS and SHBSS was the pseudo-second order model. This reveals that chemisorption is the controlling mechanism for the uptake of CR and MG (Ighalo and Eletta 2020; Jiang et al. 2017; Mahvi et al. 2020). However, this assertion is not conclusive as the pseudo-second order model has been known to over-fit adsorption data (Tran et al. 2017a). The activation energy and Gibbs free energy from the thermodynamics analysis suggest a combination of both physisorption and chemisorption mechanisms for CR and MG uptake onto PHBSS and SHBSS. This also complements the findings of the kinetics modelling.

Activation energy and thermodynamic modelling

The magnitude of the activation energy for the adsorption process can be used to differentiate between physical and chemical adsorption. The values of activation energy, E_a of the processes evaluated using the Arrhenius equation ($\mathrm{Ln}K_2 = \mathrm{Ln}A - \frac{E_a}{RT}$, where K_2 = pseudo-second-order kinetic constant (g/mg h), R = 8.314 J/mol K and A = Arrhenius factor) are shown in Table 6. Lower energies (5–40 K/Jmol) show a physical adsorption process due to their easy reversibility, with equilibrium reached quickly. Chemical adsorption requires greater interaction forces, thus larger activation energies (40–800 kJ/mol) (Boparai et al. 2011). The E_a values for the study ranged between 32 and 85 kJ/mol suggesting an interplay between physisorption and chemisorption. The thermodynamic parameters Gibbs free energy (ΔG°), enthalpy (ΔH°) and entropy (ΔS°) were evaluated at different temperatures via Eqs. 3–4 (Mesbah et al. 2020; Nwosu et al. 2019) and also summarised in Table 6.

$$\mathrm{In}K_L = \frac{\Delta S^0}{R} - \frac{\Delta H^0}{RT}, \tag{3}$$

$$\Delta G^\circ = \Delta H^\circ - T\Delta S^\circ, \tag{4}$$

where R is the universal gas constant (8.314 J/mol K), T is the absolute temperature in K, and q_e is the amount of CR and MG adsorbed per unit weight of any of the adsorbents at equilibrium concentration (mg/g) and K_L (L/mg) is the Langmuir isotherm constant. The ΔH° and ΔS° values were obtained from the linear plots of ln K_L against $1/T$ using Eq. 3. The ΔG° values were also evaluated using Eq. 4.

The positive ΔH° values indicate the endothermic nature of all the processes (Igwegbe et al. 2021). This complements the earlier findings of an increase in adsorption with temperature. The positive ΔS° values showed the good affinity of

Table 4 Isotherm parameters for CR and MG adsorption on PHBSS and SHBSS at optimum pH and 303 K

Isotherm	Adsorbate	Parameters	PHBSS	SHBSS
Langmuir	CR	Q_m (mg/g)	55.87	50.51
		b (L/mg)	0.0672	0.0739
		R_L	0.1295	0.1192
		R^2	0.9715	0.9714
	MG	Q_m (mg/g)	58.48	56.82
		b (L/mg)	0.0642	0.0650
		R_L	0.1348	0.1333
		R^2	0.9697	0.9712
Freundlich	CR	n	2.026	2.133
		K_f (L/g)	6.5796	6.6819
		R^2	0.9985	0.9979
	MG	n	1.987	1.986
		K_f (L/g)	6.5539	6.4180
		R^2	0.9988	0.9986
Temkin	CR	b_T (J/mg)	210.12	236.03
		A	0.4904	2.0671
		R^2	0.8724	0.8303
	MG	b_T (J/mg)	198.28	160.68
		A	1.2537	2.9025
		R^2	0.8951	0.9148
Elovich	CR	Q_m (mg/g)	26.738	22.624
		Ke	1.0580	1.0514
		R^2	0.8945	0.8153
	MG	Q_m (mg/g)	29.155	45.05
		Ke	1.0651	1.0236
		R^2	0.9334	0.9730
Jovanovich	CR	K_J	0.0285	0.0269
		Q_m (mg/g)	12.922	12.678
		R^2	0.828	0.8292
	MG	K_J	0.0289	0.0288
		Q_m (mg/g)	13.033	12.778
		R^2	0.8298	0.8272
Harkin-Jura	CR	A	136.99	136.99
		B	1.5890	1.6164
		R^2	0.8553	0.8605
	MG	A	138.89	131.58
		B	1.5833	1.5789
		R^2	0.8534	0.8523

Table 5 Kinetic parameters for the adsorption of CR and MG at 303 K

Kinetic model	Dye	Parameter	Adsorbent	
			PHBSS	SHBSS
Pseudo-first order	CR	K_1 (min^{-1})	0.0085	0.0069
		qe (mg/g)	1.3605	1.4077
		R^2	0.9361	0.994
	MG	K_1 (min^{-1})	0.0102	0.0063
		qe (mg/g)	1.9552	1.5382
		R^2	0.9683	0.9795
Pseudo-second order	CR	K_2 (g/mg/min)	7.1582	5.6786
		qe (mg/g)	9.9602	10.010
		R^2	0.9999	0.9999
	MG	K_2 (g/mg/min)	6.0241	4.7326
		qe (mg/g)	10.060	9.9701
		R^2	0.9999	0.9997
Intra particle diffusion	CR	k_{pi} (mg g^{-1} min$^{-0.5}$)	0.1255	0.1523
		c_i	8.72	8.4831
		R^2	0.9508	0.9679
	MG	k_{pi} (mg g^{-1} min$^{-0.5}$)	0.1593	0.1707
		c_i	8.5049	8.2345
		R^2	0.9258	0.9775

Venkateswaran 2011) and AC from grape waste (Sayğılı and Güzel 2015).

Mechanism of dye uptake

Based on the findings on the modelling studies, the possible mechanism of CR and MG uptakes onto PHBSS and SHBSS are discussed in this section. It has already been revealed that a combination of both chemisorption and physisorption is at play for the dye uptake. This section attempts to narrow down the specific forces in play for the pollutant uptake. The pKa of CR is 4.1 (Yaneva and Georgieva 2012) and it is protonated to its cationic (positively charged) form below this pH. At low pH, CR uptake is likely due to electrostatic attraction between the dye and the negatively charged surface of the adsorbent. At higher pH, the CR is in the neutral form in solution and the major uptake mechanisms are hydrogen bonds and pore diffusion. Hydrogen bonds are weak partial intermolecular bonds and a special type of dipole–dipole moment (Steiner 2002). The pKa of MG is 10.3 (Sartape et al. 2017). Below this value, it is protonated and exists in its cationic (positively charged) form. Electrostatic attraction between MG and the negatively charged surface of the adsorbent is a major mechanism of uptake. Weak hydrogen bonds and pore diffusion also contribute to the uptake of MG (to a lesser extent). Hydrogen bonds are possible as the alkyl hydrogens on the adsorbate can interact with molecules on the adsorbent functional groups such

the PHBSS and SHBSS for CR and MG during the adsorption process. Negative ΔG^o values indicate that the processes were spontaneous (Hevira et al. 2021; Igwegbe et al. 2015). The intermediate values of the magnitude of ΔG^o also suggest a combination of physical and chemical adsorption in the uptakes of both CR and MG (Eletta et al. 2020a). Spontaneous and endothermic adsorption has been reported for cationic dyes (Rhodamine B and methylene blue) from aqueous solution using treated fruit waste (Parimaladevi and

Table 6 Thermodynamic parameters and activation energies of the process

Dye	Adsorbent	ΔH^o (KJ/mol)	ΔS^o (J/K/mol)	ΔG^o (KJ/mol)			Activation energy, E_a (kJ/mol)
				303 K	313 K	323 K	
CR	PHBSS	28.268	70.503	−21.334	−22.039	−22.744	38.5975
	SHBSS	15.572	27.104	−8.197	−8.468	−8.739	52.5740
MG	PHBSS	16.761	35.650	−10.785	−11.142	−11.498	85.7830
	SHBSS	20.469	40.705	−12.313	−12.720	−13.127	32.8482

as oxygen (confirmed from the FTIR). Functional groups like C=O, C–O and –OH have been confirmed from the FTIR analysis. Both CR and MG are polycyclic aromatic compounds (as seen from Fig. 1a–b). This means that they contain several benzene rings in their structure. These rings are electron-rich zones that could induce a donor–acceptor relationship and a stacking effect of the dyes onto the adsorbent (Aniagor et al. 2021; Oba et al. 2021). Therefore, π–π electron–donor interaction is also a contributing adsorption mechanism. In summary, the mechanism of CR and MG uptakes was by a combination of electrostatic attraction, π–π electron–donor interaction, hydrogen bonds and pore diffusion. A summary of the dye adsorption mechanism is presented in Fig. 11.

Comparison with other adsorbents

It is important to compare the performance of the adsorbent with other materials for the uptake of CR and MG (Swan and Zaini 2019). Such a comparison is presented in Table 7. The pH and temperature are also reported as they are important variables that affect the solution chemistry which subsequently influences the adsorption capacity value (Ighalo and Adeniyi 2020d; Ighalo et al. 2020). The adsorption capacity of PHBSS and SHBSS to CR was 55.87 and 50.51 mg/g respectively while for MG was 58.48 and 56.82 mg/g respectively. It can be observed from Table 7 that the activated carbon from *Hevea brasiliensis* seed shells has intermediate adsorption capacities for CR and MG uptake in comparison to other adsorbents. It is also observed that the adsorbent activated with phosphoric acid (PHBSS) has a better performance than that activated with sodium chloride (SHBSS).

Fig. 11 Summary of adsorption mechanism for CR and MG onto the adsorbent (Tran et al. 2017b)
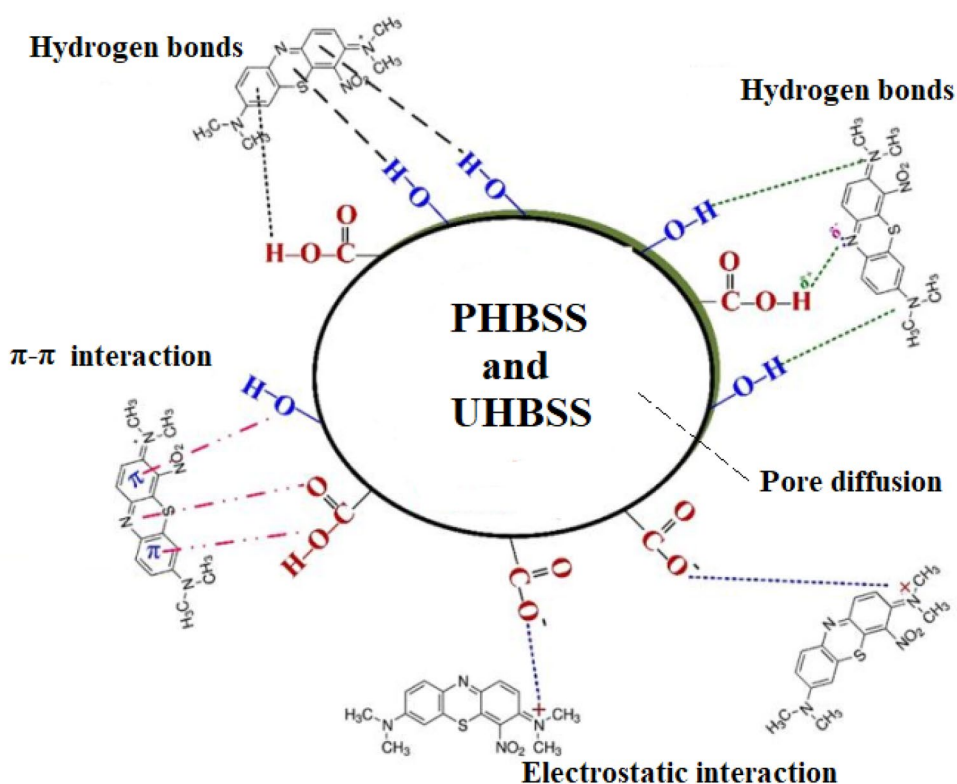
Table 7 Comparison of various adsorbents for CR and MG uptake

Material	Dye	Q_e (mg/g)	Temp (K)	pH	References
AC from grape waste	MG	666.7	328	4.00	Sayğılı and Güzel (2015)
AC from bamboo	MG	263.6	303	4.00	Hameed and El-Khaiary (2008)
AC from jute fibres	MG	136.6	303	10.0	Porkodi and Kumar (2007)
PHBSS	**MG**	58.48	**303**	**10.0**	**Current study**
SHBSS	**MG**	56.82	**303**	**10.0**	**Current study**
Fe–Zn bimetallic nanoparticles	MG	21.74	303	9.00	Gautam et al. (2015)
Neem sawdust	MG	4.354	298	7.20	Khattri and Singh (2009)
AC from grape waste	CR	454.6	328	6.95	Sayğılı and Güzel 2015)
Pine bark AC (Fenton functionalised)	CR	111.0	328	2.00	Omorogie et al. (2019)
Pine bark AC (microwave activated)	CR	107.2	328	2.00	Omorogie et al. (2019)
Pine bark AC	CR	70.20	328	2.00	Omorogie et al. (2019)
Sycamore bark AC	CR	56.43	313	–	Cong et al. (2017)
PHBSS	**CR**	55.87	**303**	**2.00**	**Current study**
SHBSS	**CR**	50.51	**303**	**2.00**	**Current study**
Acid-treated pine cone	CR	40.19	343	3.55	Dawood and Sen (2012)
Pine cone	CR	32.65	343	3.55	Dawood and Sen (2012)
Fe–Zn bimetallic nanoparticles	CR	28.58	303	4.00	Gautam et al. (2015)
Walnut shell	CR	22.90	318	6.40	Liu et al. (2019)
Acid-activated red mud	CR	7.080	298	7.00	Tor and Cengeloglu (2006)

Rows in bold represent results of the current study

Conclusion

Hevea brasiliensis seed shells (HBSS) activated with H_3PO_4 and NaCl were explored for the removal of CR and MG from aqueous solutions. The adsorbent had excellent physicochemical properties (specific surface area, iodine number, bulk density and fixed carbon content) for the specific application in question. Potassium oxide (K_2O), iron oxide (Fe_2O_3), phosphorus oxide (P_2O_5) and calcium oxide (CaO) were the major inorganic components in both PHBSS and SHBSS while other species were present in smaller amounts. There were numerous cavities and undulations on the surface of both AC thereby giving it a heterogeneous aspect. The uptake of both dyes was optimum at 0.3 mm particle size, 2 g/L adsorbent dosage and 100 mg/L initial dye concentration. CR and MG uptake was highest at pH 2 and 10 respectively. The adsorption capacity of PHBSS and SHBSS to CR was 55.87 and 50.51 mg/g and 58.48 and 56.82 mg/g respectively for MG. The study observed that the uptake of both dyes by both adsorbents was best fit to the Freundlich isotherm and the pseudo-second order kinetic models. Thermodynamics modelling revealed that the processes were spontaneous and endothermic. The mechanism of CR and MG uptake was by a combination of electrostatic attraction, π-π electron–donor interaction, hydrogen bonds and pore diffusion. Furthermore, H_3PO_4 was a better activating agent for HBSS than NaCl given the current application.

Declarations

Conflict of interest The authors declare that there are no conflicts of interest.

Compliance with ethical standards This article does not contain any studies involving human or animal subjects.

References

Abdullahi AA, Ighalo JO, Ajala OJ, Ayika S (2020) Physicochemical analysis and heavy metals remediation of pharmaceutical industry effluent using bentonite clay modified by H_2SO_4 and HCl. J Turk Chem Soc Sect A 7:727–744. https://doi.org/10.18596/jotcsa.703913

Ahmad R, Kumar R (2010) Adsorption studies of hazardous malachite green onto treated ginger waste. J Environ Manag 91:1032–1038

Ahmadi S, Igwegbe CA (2018) Adsorptive removal of phenol and aniline by modified bentonite: adsorption isotherm and kinetics study. Appl Water Sci 8:170–178

Ahmadi S, Igwegbe CA (2020) Removal of methylene blue on zinc oxide nanoparticles: nonlinear and linear adsorption isotherms

and kinetics study. Sigma: J Eng Natl Sci/Mühendislik ve Fen Bilimleri Dergisi 38

Ahmadi S, Mohammadi L, Rahdar A, Rahdar S, Dehghani R, Igwegbe CA, Kyzas GZ (2020) Acid dye removal from aqueous solution by using neodymium (III) oxide nanoadsorbents. Nanomaterials 10:556–582

Aljeboree AM, Alshirifi AN, Alkaim AF (2017) Kinetics and equilibrium study for the adsorption of textile dyes on coconut shell activated carbon. Arab J Chem 10:S3381–S3393. https://doi.org/10.1016/j.arabjc.2014.01.020

Aniagor CO, Igwegbe CA, Ighalo JO, Oba SN (2021) Adsorption of doxycycline from aqueous media: a review. J Mol Liq 334:116124. https://doi.org/10.1016/j.molliq.2021.116124

Balarak D, Chandrika K, Igwegbe CA, Ahmadi S, Umembamalu CJ (2020) Biosorption of phenol using modified barley husk: Studies on equilibrium isotherm, kinetics, and thermodynamics of interactions. Sigma: J Eng Natl Sci/Mühendislik ve Fen Bilimleri Dergisi 38

Balarak D, Ganji F, Rajiv P, Igwegbe C, Ighalo JO (2021a) Ultimate eradication of acid orange 7 from contaminated liquid via synthesised mesoporous goethite. J Turk Chem Soc Sect B Chem Eng 4:13–26

Balarak D, Zafariyan M, Igwegbe CA, Onyechi KK, Ighalo JO (2021b) Adsorption of acid blue 92 dye from aqueous solutions by single-walled carbon nanotubes: isothermal, kinetic, and thermodynamic studies. Environ Process 8:1–20

Baseri JR, Palanisamy P, Sivakumar P (2012) Preparation and characterization of activated carbon from *Thevetia peruviana* for the removal of dyes from textile waste water. Adv Appl Sci Res 3:377–383

Blagodatsky S, Xu J, Cadisch G (2016) Carbon balance of rubber (*Hevea brasiliensis*) plantations: a review of uncertainties at plot, landscape and production level. Agric Ecosyst Environ 221:8–19

Boparai HK, Joseph M, O'Carroll DM (2011) Kinetics and thermodynamics of cadmium ion removal by adsorption onto nano zerovalent iron particles. J Hazard Mater 186:458–465

Cheng W, Wang S-G, Lu L, Gong W-X, Liu X-W, Gao B-Y, Zhang H-Y (2008) Removal of malachite green (MG) from aqueous solutions by native and heat-treated anaerobic granular sludge. Biochem Eng J 39:538–546

Coates J (2010) Interpretation of infrared spectra, a practical approach. In: Encyclopaedia of analytical chemistry: applications, theory and instrumentation. Wiley, Chichester

Cong L, Lingling F, Xinlai W, Jie J, Ke W (2017) Study on the Adsorption Characteristics of Congo Red by Sycamore Bark Activated Carbon. Paper presented at the Proceedings of the 11th International Scientific and Practical Conference, Rezekne, Latvia, June 15–17, 2017

Dahiru M, Zango ZU, Haruna MA (2018) Cationic dyes removal using low-cost banana peel biosorbent. Am J Mater Sci 8:32–38

Dawood S, Sen TK (2012) Removal of anionic dye Congo red from aqueous solution by raw pine and acid-treated pine cone powder as adsorbent: equilibrium, thermodynamic, kinetics, mechanism and process design. Water Res 46:1933–1946

De Gisi S, Lofrano G, Grassi M, Notarnicola M (2016) Characteristics and adsorption capacities of low-cost sorbents for wastewater treatment: a review. Sustain Mater Technol 9:10–40

Devi BV, Jahagirdar A, Ahmed MZ (2012) Adsorption of chromium on activated carbon prepared from coconut shell. Int J Eng Res Appl 2:364–370

Devi AP, Mishra PM (2019) Biosorption of dysprosium (III) using raw and surface-modified bark powder of *Mangifera indica*: isotherm, kinetic and thermodynamic studies. Environ Sci Pollut Res 26:6545–6556

Egwaikhide PA, Akporhonour EE, Okieimen FE (2007) Utilization of coconut fibre carbon in the removal of soluble petroleum fraction polluted water. Int J Phys Sci 2:47–49

Ekpete O, Horsfall M (2011) Preparation and characterization of activated carbon derived from fluted pumpkin stem waste (*Telfairia occidentalis* Hook F). Res J Chem Sci 1:10–17

Eletta AAO, Tijani IO, Ighalo JO (2020a) Adsorption of Pb(II) and phenol from wastewater using silver nitrate modified activated carbon from groundnut (*Arachis hypogaea* L) shells. West Indian J Eng 43:26–35

Eletta OAA, Adeniyi AG, Ighalo JO, Onifade DV, Ayandele FO (2020b) Valorisation of cocoa (*Theobroma cacao*) pod husk as precursors for the production of adsorbents for water treatment. Environ Technol Rev 9:20–36. https://doi.org/10.1080/21622515.2020.1730983

Eletta OAA, Ayandele FO, Ighalo JO (2021) Adsorption of Pb(II) and Fe(II) by mesoporous composite activated carbon from tithonia diversifolia stalk and theobroma cacao pod. Biomass Conver Biorefin. https://doi.org/10.1007/s13399-021-01699-0

Elovich SY, Larinov OG (1962) Theory of adsorption from solutions of non electrolytes on solid (I) equation adsorption from solutions and the analysis of its simplest form, (II) verification of the equation of adsorption isotherm from solutions. Izvestiya Akademii Nauk SSSR, Otdelenie Khimicheskikh Nauk 2:209–216

Freundlich H (1906) Over the adsorption in solution. J Phys Chem 57:1100–1107

Gautam RK, Rawat V, Banerjee S, Sanroman MA, Soni S, Singh SK, Chattopadhyaya MC (2015) Synthesis of bimetallic Fe–Zn nanoparticles and its application towards adsorptive removal of carcinogenic dye malachite green and Congo red in water. J Mol Liq 212:227–236

Granados-Correa F, Vilchis-Granados J, Jiménez-Reyes M, Quiroz-Granados LA (2013) Adsorption behaviour of La(III) and Eu(III) Ions from aqueous solutions by hydroxyapatite: kinetic, isotherm, and thermodynamic studies. J Chem. https://doi.org/10.1155/2013/751696

Gregg SJ, Sing KSW (1982) Adsorption, surface area and porosity, 2nd edn. Academic Press Inc, New York

Gupta V (2009) Application of low-cost adsorbents for dye removal—a review. J Environ Manag 90:2313–2342. https://doi.org/10.1016/j.jenvman.2008.11.017

Hameed B, El-Khaiary M (2008) Equilibrium, kinetics and mechanism of malachite green adsorption on activated carbon prepared from bamboo by K_2CO_3 activation and subsequent gasification with CO_2. J Hazard Mater 157:344–351

Han Y, Cao X, Ouyang X, Sohi SP, Chen J (2016) Adsorption kinetics of magnetic biochar derived from peanut hull on removal of Cr (VI) from aqueous solution: effects of production conditions and particle size. Chemosphere 145:336–341. https://doi.org/10.1016/j.chemosphere.2015.11.050

Hessel C, Allegre C, Maisseu M, Charbit F, Moulin P (2007) Guidelines and legislation for dye house effluents. J Environ Manag 83:171–180

Hevira L, Zilfa R, Ighalo JO, Zein R (2020) Biosorption of indigo carmine from aqueous solution by terminalia catappa shell. J Environ Chem Eng 8:104290. https://doi.org/10.1016/j.jece.2020.104290

Hevira L, Zilfa R, Ighalo JO, Aziz H, Zein R (2021) Terminalia catappa shell as low-cost biosorbent for the removal of methylene blue from aqueous solutions. J Ind Eng Chem 97:188–199. https://doi.org/10.1016/j.jiec.2021.01.028

Ho YS, McKay G (1999) Pseudo-second order model for sorption processes. Process Biochem 34:451–465. https://doi.org/10.1016/S0032-9592(98)00112-5

Ho YS, Ng JCY, McKay G (2000) Kinetics of pollutant sorption by biosorbents: review. Sep Purif Methods 29:189–232

Ighalo JO, Adeniyi AG (2020a) Adsorption of pollutants by plant bark derived adsorbents: an empirical review. J Water Process Eng 35:101228. https://doi.org/10.1016/j.jwpe.2020.101228

Ighalo JO, Adeniyi AG (2020b) A comprehensive review of water quality monitoring and assessment in Nigeria. Chemosphere 260:127569. https://doi.org/10.1016/j.chemosphere.2020.127569

Ighalo JO, Adeniyi AG (2020c) A Mini-review of the morphological properties of biosorbents derived from plant leaves. SN Appl Sci 2:509. https://doi.org/10.1007/s42452-020-2335-x

Ighalo JO, Adeniyi AG (2020d) Mitigation of diclofenac pollution in aqueous media by adsorption. ChemBioEng Rev 7:50–64. https://doi.org/10.1002/cben.201900020

Ighalo JO, Eletta AAO (2020) Response surface modelling of the biosorption of Zn(II) and Pb(II) onto micropogonias undulates scales: box-behnken experimental approach. Appl Water Sci 10:197–209. https://doi.org/10.1007/s13201-020-01283-3

Ighalo JO, Ajala JO, Umenweke G, Ogunniyi S, Adeyanju CA, Igwegbe CA, Adeniyi AG (2020) Mitigation of clofibric acid pollution by adsorption: a review of recent developments. J Environ Chem Eng 8:104264. https://doi.org/10.1016/j.jece.2020.104264

Ighalo JO, Adeniyi AG, Igwegbe CA (2021) 3D reconstruction and morphological analysis of electrostimulated hyperthermophile biofilms of *Thermotoga neapolitana*. Biotechnol Lett 43:1303–1309. https://doi.org/10.1007/s10529-021-03123-z

Igwegbe C, Onyechi P, Onukwuli O (2015) Kinetic, isotherm and thermodynamic modelling on the adsorptive removal of malachite green on *Dacryodes edulis* seeds. J Sci Eng Res 2:23–39

Igwegbe CA, Onyechi PC, Onukwuli OD, Nwokedi IC (2016) Adsorptive treatment of textile wastewater using activated carbon produced from *Mucuna pruriens* seed shells. World J Eng Technol 4:21–37. https://doi.org/10.4236/wjet.2016.41003

Igwegbe CA, Onukwuli OD, Ighalo JO, Okoye PU (2020a) Adsorption of cationic dyes on *Dacryodes edulis* seeds activated carbon modified using phosphoric acid and sodium chloride. Environ Process 7:1151–1171

Igwegbe CA, Onukwuli OD, Onyechi KK, Ahmadi S (2020b) Equilibrium and kinetics analysis on Vat Yellow 4 uptake from aqueous environment by modified rubber seed shells: nonlinear modelling. J Mater Environ Sci 11:1424–1444

Igwegbe CA, Oba SN, Aniagor CO, Adeniyi AG, Ighalo JO (2021) Adsorption of ciprofloxacin from water: a comprehensive review. J Ind Eng Chem 93:57–77. https://doi.org/10.1016/j.jiec.2020.09.023

Jeirani Z, Niu CH, Soltan J (2017) Adsorption of emerging pollutants on activated carbon. Rev Chem Eng 33:491–522. https://doi.org/10.1515/revce-2016-0027

Jiang F, Dinh DM, Hsieh Y-L (2017) Adsorption and desorption of cationic malachite green dye on cellulose nanofibril aerogels. Carbohydr Polym 173:286–294

Jura G, Harkins WD (1943) A new adsorption isotherm which is valid over a very wide range of pressure. J Chem Phys 11:430–431

Khattri S, Singh M (2009) Removal of malachite green from dye wastewater using neem sawdust by adsorption. J Hazard Mater 167:1089–1094

Kumar KV (2007) Optimum sorption isotherm by linear and non-linear methods for malachite green onto lemon peel. Dyes Pigments 74:595–597

Kumari S, Khan AA, Chowdhury A, Bhakta AK, Mekhalif Z, Hussain S (2020) Efficient and highly selective adsorption of cationic dyes and removal of ciprofloxacin antibiotic by surface modified nickel sulfide nanomaterials: kinetics, isotherm and adsorption mechanism. Colloids Surf Physicochem Eng Aspects 586:124264

Lagergren S, Svenska BK (1898) On the theory of so-called adsorption of dissolved substances. R Swed Acad Sci Doc 24:1–13

Langmuir I (1918) The adsorption of gases on plane surfaces of glass, mica and platinum. JACS 40:1361–1403

Liu M, Li X, Du Y, Han R (2019) Adsorption of methyl blue from solution using walnut shell and reuse in a secondary adsorption for Congo red. Bioresour Technol Rep 5:238–242

Louis NSM, Thomas S (2013) Activated carbon from tapioca leaves for treating dye waste. Water Toxicol Environ Health Sci 5:131–137

Mahvi AH, Rahdar A, Igwegbe CA, Rahdar S, Ahmadi S (2020) Fluoride removal from aqueous solutions by zinc oxide nanoparticles. Fluoride 53:531–541

Mesbah M, Hamedshahraki S, Ahmadi S, Sharifi M, Igwegbe CA (2020) Hydrothermal synthesis of LaFeO$_3$ nanoparticles adsorbent: characterization and application of error functions for adsorption of fluoride. MethodsX 7:100786

Misra DN (1973) Jovanovich adsorption isotherm for heterogeneous surfaces. J Colloid Interface Sci 43:85–88

Nwabanne JT, Igbokwe PK (2012) Thermodynamic and kinetic behaviors of lead (II) adsorption on activated carbon derived from Palmyra palm nut. Int J Appl Sci Technol 2:245–254

Nwosu FO, Ajala OJ, Okeola FO, Adebayo SA, Olanlokun OK, Eletta OAA (2019) Adsorption of chlorotriazine herbicide onto unmodified and modified kaolinite: equilibrium, kinetic and thermodynamic studies. Egypt J Aquat Res 45:99–107. https://doi.org/10.1016/j.ejar.2019.05.005

Oba SN, Ighalo JO, Aniagor CO, Igwegbe CA (2021) Removal of ibuprofen from aqueous media by adsorption: a comprehensive review. Sci Total Environ 780:146608. https://doi.org/10.1016/j.scitotenv.2021.146608

Omorogie MO, Babalola JO, Olatunde AM, Alimi T, John KI, Adegboyega SA, Abesa SK (2019) Microwave-synthesized and Fenton-functionalized *Pinus sylvestris* bark activated carbon/metal oxides for the effective uptake of tetracycline and congo red dye. Biomass Convers Biorefin. https://doi.org/10.1007/s13399-019-00460-y

Onyechi C (2014) Textile wastewater treatment using activated carbon from agro wastes. M. Eng. Thesis, Department of Chemical Engineering, Nnamdi Azikiwe University, Awka

Parimaladevi P, Venkateswaran V (2011) Adsorption of cationic dyes (rhodamine B and methylene blue) from aqueous solution using treated fruit waste. J Appl Technol Environ Sanit 1:285–293

Porkodi K, Kumar KV (2007) Equilibrium, kinetics and mechanism modeling and simulation of basic and acid dyes sorption onto jute fiber carbon: eosin yellow, malachite green and crystal violet single component systems. J Hazard Mater 143:311–327

Rehman MZU, Aslam Z, Shawabkeh RA, Hussein IA, Mahmood N (2020) Concurrent adsorption of cationic and anionic dyes from environmental water on amine functionalized carbon. Water Sci Technol. https://doi.org/10.2166/wst.2020.119

Rengaraj S, Moon S-H, Sivabalan R, Arabindoo B, Murugesan V (2002) Agricultural solid waste for the removal of organics: adsorption of phenol from water and wastewater by palm seed coat activated carbon. Waste Manag (oxford) 22:543–548

Saka C (2012) BET, TG–DTG, FT-IR, SEM, iodine number analysis and preparation of activated carbon from acorn shell by chemical activation with ZnCl$_2$. J Anal Appl Pyrolysis 95:21–24

Sartape AS, Mandhare AM, Jadhav VV, Raut PD, Anuse MA, Kolekar SS (2017) Removal of malachite green dye from aqueous solution with adsorption technique using *Limonia acidissima* (wood apple) shell as low cost adsorbent. Arab J Chem 10:S3229–S3238

Sayğılı H, Güzel F (2015) Performance of new mesoporous carbon sorbent prepared from grape industrial processing wastes for malachite green and Congo red removal. Chem Eng Res Des 100:27–38

Shafeeyan MS, Wan Daud WMA, Houshmand A, Shamiri A (2010) A review on surface modification of activated carbon adsorption. J Anal Appl Pyrolysis 89:143–151

Sharma P, Kaur H, Sharma M, Sahore V (2011) A review on applicability of naturally available adsorbents for the removal of hazardous dyes from aqueous waste. Environ Monit Assess 183:151–195

Souza EC, Pimenta AS, Silva AJF, Nascimento PFP, Ighalo JO (2021) HNO3-treated eucalyptus charcoal: a sustainable biosorbent for removing heavy metals from aqueous solutions. Biomass Conv Biorefin. https://doi.org/10.1007/s13399-021-01431-y

Steiner T (2002) The hydrogen bond in the solid state. Angew Chem Int Ed 41:48–76

Sud D, Mahajan G, Kaur M (2008) Agricultural waste material as potential adsorbent for sequestering heavy metal ions from aqueous solutions—a review. Bioresour Technol 99:6017–6027. https://doi.org/10.1016/j.biortech.2007.11.064

Swan NB, Zaini MAA (2019) Adsorption of malachite green and Congo red dyes from water: recent progress and future outlook. Ecol Chem Eng 26:119–132

Temkin M, Pyzhev V (1940) Recent modifications to langmuir isotherms. Acta Physiochim URSS 12:217–222

Tor A, Cengeloglu Y (2006) Removal of congo red from aqueous solution by adsorption onto acid activated red mud. J Hazard Mater 138:409–415. https://doi.org/10.1016/j.jhazmat.2006.04.063

Tran HN, You S-J, Hosseini-Bandegharaei A, Chao H-P (2017a) Mistakes and inconsistencies regarding adsorption of contaminants from aqueous solutions: a critical review. Water Res 120:88–116. https://doi.org/10.1016/j.watres.2017.04.014

Tran HN, You S-J, Nguyen TV, Chao H-P (2017b) Insight into the adsorption mechanism of cationic dye onto biosorbents derived from agricultural wastes. Chem Eng Commun 204:1020–1036

Uddin MK (2017) A review on the adsorption of heavy metals by clay minerals, with special focus on the past decade. Chem Eng J 308:438–462

Wan Ngah WS, Ariff NFM, Hashim A, Hanafiah MAKM (2010) Malachite green adsorption onto chitosan coated bentonite beads: isotherms, kinetics and mechanism. Clean: Soil, Air, Water 38:394–400

Weber W, Morris J (1963) Kinetics of adsorption on carbon from solution. J Sanit Eng Div Am Soc Civ Eng 89:31–60

Yaneva ZL, Georgieva NV (2012) Insights into congo red adsorption on agro-industrial materials- spectral, equilibrium, kinetic, thermodynamic, dynamic and desorption studies a review. Int Rev Chem Eng 4:127–146

Zhang F, Ma B, Jiang X, Ji Y (2016) Dual function magnetic hydroxyapatite nanopowder for removal of malachite green and Congo red from aqueous solution. Powder Technol 302:207–214